EUROPEAN ORGANIZATION FOR NUCLEAR RESEARCH

A MEASUREMENT OF THE POLARIZATION PARAMETER IN BACKWARD π^-p ELASTIC SCATTERING AT 3.5 GeV/c

R. Birsa, F. Bradamante, S. Conetti*), C. Daum**), G. Fidecaro, M. Fidecaro, M. Giorgi, A. Penzo, L. Piemontese, P. Schiavon, A. Vascotto, and A. Villari

CERN-Trieste***) High-Energy Group

ABSTRACT

The polarization parameter has been measured for π^-p elastic scattering in the backward region at 3.5 GeV/c incident momentum. The experimental set-up consisted of a polarized target in a spectrometer magnet, hodoscopes and wire spark chambers. Data are presented for the range $-0.95 < u \leq -0.19$ GeV^2. An isospin analysis has been carried out to separate the $I_u = \frac{1}{2}$ and $I_u = \frac{3}{2}$ contributions.

Geneva - 30 August 1976

(Submitted to Nuclear Physics B)

---

*) Now at McGill University, Montreal, Canada.

**) Visitor from the Foundation for Fundamental Research of Matter (FOM), The Netherlands.

***) Istituto di Fisica dell'Università di Trieste and Istituto Nazionale di Fisica Nucleare, Sezione di Trieste, Italy.

1. INTRODUCTION

We have measured the polarization P in the backward scattering reactions $\pi^- p \to p\pi^-$ and $\pi^- p \to \Sigma^- K^+$ at an incident pion momentum of 3.5 GeV/c. In this paper we report our results on the elastic scattering.

The experiment was the continuation of a previous one, in which we measured the polarization for the reactions $\pi^+ p \to p\pi^+$ [1] and $\pi^+ p \to \Sigma^+ K^+$ [2].

Data already exist at this energy on differential cross-sections for the reactions $\pi^- p \to p\pi^-$ [3], $\pi^+ p \to p\pi^+$ [3,4], and $\pi^- p \to n\pi^0$ [5]. These new data on polarizations complete the picture of backward pion-proton scattering at 3.5 GeV/c. We have therefore performed at this energy a model-independent isospin analysis of the scattering amplitudes similar to that of Barger and Olsson[6] for the data at 6 GeV/c.

Our data, when compared with those from experiments at different energies[7,8], show that the polarization is still varying drastically with energy; in particular, data at 3.5 and 6 GeV/c are very different, while for the positive pion scattering the polarizations at these energies are almost identical[1,9].

Backward pion-proton elastic scattering is conventionally considered to be dominated by the exchange of baryon quantum numbers[10]. However, in the last years all models based on Regge parametrization of baryon exchange have failed to correctly predict new data: in particular, the polarization data in the pion-proton elastic reaction[1,7,9,11] have been in contradiction with the predictions of all previous models[12]. Various new models have been proposed to explain these data and new polarization data in $\pi^- p$ elastic scattering[7]: their general tendency is either to drop the condition of Regge behaviour for some amplitudes while retaining it for others, or to add to the Regge term a "background" amplitude.

2. EXPERIMENTAL APPARATUS

The main difficulty of the experiment consisted in the necessity of selecting a reaction with very low cross section ($\sim$ 1 μb) in the presence of a large background, mainly due to forward inelastic reactions taking place on the complex nuclei of the polarized target (PT), with one secondary particle deviated by the PT magnet field into the solid angle of the backward scattered pion. This selection has been achieved in both of our elastic scattering experiments by measuring the directions of the two outgoing particles and the momentum of the backward meson in the fringing field of the PT magnet. There are, however, considerable differences in the two experiments:

- In both experiments the two reactions were measured simultaneously, but for π^- beam the backward K^+ and π^- have a different charge; hence one particle, in our case the π^-, was defocused by the PT magnet. This prevented us from

measuring the elastic reaction up to the kinematical limit $u - u_0 = 0$ and considerably increased the solid angle covered by our detectors.

- A new PT magnet has been used which has three times the bending power than that in the π^+ experiment[1], and the number of spark chambers used in the magnetic field region has been increased, thus reducing by about a factor of 3 the error in the measurement of the meson momentum.
- The spark chamber telescope in the forward arm has been replaced by a pair of scintillation counter hodoscopes which give less information (no direction measured) but can stand a higher rate.
- The trigger has been rearranged; it has not been possible to cover the angular region of the forward proton with a Čerenkov counter to cut down on triggers with forward pions, but the veto counter around the target has been improved.

2.1 Layout

The experimental layout is shown in Fig. 1. Figure 2 gives a more detailed view of the target region. Only those parts of the apparatus which are relevant to the elastic reaction will be described.

The incident pion beam was focused on the polarized target and defined by the four scintillation counters B_1 - B_4 and by the Čerenkov counter $\check{C}_1$. The backward scattered pion was detected by counters M_1, M_4, M_5, and M_6, and its trajectory measured by a set of eight spark chambers S_1-S_8.

The forward recoil proton was both detected and measured by the pair of hodoscopes R_2 (horizontal) and R_3 (vertical).

2.2 Beam

The negative incident beam (m_9) 52.5 m long, derived from an internal target of the CERN Proton Synchrotron (PS), was momentum and mass selected and focused onto the target on a spot of 7 mm diameter.

The beam divergence at the target was ±11 mrad in the horizontal and ±7 mrad in the vertical plane, and the accepted momentum bite was ±1%.

The incident beam was defined by the counters B_1, B_2, B_3, B_4, and $\check{C}_1$. Counters B_1 and B_2 detected the total beam, while the hole counter B_3 and B_4 imposed the condition of focusing onto the target, and the threshold Čerenkov counter $\check{C}_1$ filled with ethylene at 7 kg/cm^2 identified the incoming pions.

The rate was about 10^6 incident pions per burst of 400 msec duration. About 81% of the total beam was focused on the polarized target.

2.3 Target

The polarized proton target has been provided by the CERN Polarized Target Group. The target itself was a propanediol sample[13] of 35 mm length and 16 mm diameter maintained at the temperature of 0.5 K in a magnetic field of 2.502 T.

The polarization was measured by integrating numerically, with an on-line computer, the nuclear magnetic resonance signals for natural and dynamically enhanced polarization. The free proton polarization was typically 84%. The target polarization was frequently reversed during the data taking in order to minimize the systematic error due to variation of efficiency of the apparatus with time.

A hydrogen-free carbon target[1] has been used to measure the background due to events on complex nuclei which would satisfy the event selection procedure.

2.4 Magnet

The PT magnet used was a C-type spectrometer magnet which has been especially modified for this experiment. Coils and tapered pole faces have been added in order to provide a highly homogeneous ($\pm 2.5 \times 10^{-4}$) magnetic field of 2.502 T in the target region. The field had azimuthal symmetry, and is represented in Fig. 3, where the positions of the spark chambers are also indicated. The bending power of the magnet in the median plane was 0.93 T•m from the centre of magnet and 0.77 T•m from the first spark chamber to the region of zero field.

The vertical and radial components of the magnetic field have been accurately measured on a dense set of points in the volume of interest. After checking the azimuthal symmetry, we have parametrized the field as the super-position of the fields produced by 34 pairs of concentric Helmholtz coils.

2.5 Counters and trigger logics

The incident beam was defined by the coincidence $B_1 B_2 \bar{C}_1 \bar{B}_3 B_4$. The forward recoil proton was detected in the two hodoscopes R_2 and R_3. Hodoscope R_2 consisted of 15 scintillator strips, each 20 cm high, 2.5 cm wide, and 1 cm thick. The strips were connected to four photomultipliers by a coded system of light-guides (Fig. 4) which identified each strip uniquely by the pattern of PM's which gave a signal. Since one of the PMs was connected to the eight strips near the beam line, it was possible to divide the forward angular region at the trigger level into two subsets, "low $|u|$" and "large $|u|$" regions, which were separately in coincidence with the corresponding counters in the scattered pion arm.

Counter R_3 was a hodoscope made of 15 strips of wedge-shaped scintillator, each covering a 2° azimuthal angle interval around the beam line. The scintillator thickness was 2 cm, and was covered by one to four light-guides, each 0.5 cm thick. Again only four photomultipliers were connected to the 15 scintillator strips.

In the backward arm, counters M_4 and M_5-M_6 detected the scattered pions. They were 1 m^2 counters, each made of ten strips of scintillator of 1 cm thickness, connected via lamelled light-guides to one 58 AVP. Counters M_5 and M_6 had PMs on opposite sides, which allowed delays due to light propagation in the scintillators to be compensated at the trigger stage by using a mean timer circuit. A tight time-of-flight window accepting only $\beta \simeq 1$ particles was used.

Counter M_1, at 5 cm distance from the centre of the target, was put in coincidence to select only those reactions which took place in the target. The trigger logic was completed by a set of veto counters to cut out unwanted inelastic reactions. Čerenkov counters $\check{C}_2$ (ethylene at 17 kg/cm^2) and $\check{C}_3$ (ethylene at 7 kg/cm^2) vetoed non-interacting beam particles and reactions with pions scattered at small angles. The nose of the cryostat, which contained the target, was surrounded by the cylindrical counter B_5, apart from some holes corresponding to the angular regions of the accepted reactions. Counter B_5 consisted of two concentric cylinders of scintillator, between which a 4 mm thick layer of tantalum was inserted to convert γ-rays from π^0 decay. This counter reduced the triggering rate by a factor of $\sim$ 5.5. Finally, counters M_7 and M_8 limited the acceptance of counters M_3-M_6, and also cut triggers due to inelastic reactions.

Under these conditions the rates were $\sim$ 2.3 tr/burst for "low $|u|$" and $\sim$ 5 tr/burst for "high $|u|$" triggers, to which about 5.5 tr/burst had to be added for the $\pi^- p \to \Sigma^- K^+$ reaction, which was accepted simultaneously. To reduce the over-all rate we suppressed the "high $|u|$" elastic trigger by a factor of 2 using an electronic time gate.

2.6 Spark chambers

Chambers S_5-S_8 were large (3 × 1 m^2), thin-gap (10 mm) wire spark chambers with orthogonal aluminium wires in the two electrodes and magnetostrictive read-out[14]. Chambers S_1-S_4 were cylindrical spark chambers with horizontal and vertical wires and magnetostrictive read-out, built along the same principles as the chamber described by Bradamante et al.[15]. Chambers S_1 and S_2 each had horizontal and vertical wires, which consisted of 0.5 mm wide, 0.035 mm thick copper strips printed on a 0.1 mm thick kapton foil. Chamber S_3 had horizontal wires made of printed circuit, whereas the vertical wires were Cu-Be wires of 0.1 mm diameter, and S_4 had only vertical wires of the same type as those of S_3 vertical. Printed circuits have been used to extend the wires of the chambers to a region where the magnetic field was low enough to allow a magnetostrictive read-out system to operate reliably. This procedure somewhat spoiled the intrinsic resolution of the spark chambers; while the spark location error is of about 0.4 mm for chambers S_5-S_8, it is $\sim$ 0.6 mm for S_1 and S_2, $\sim$ 0.8 mm for S_3, and $\sim$ 1.7 mm for S_4.

The relative alignment of the chambers has been accurately determined by measuring straight tracks in special runs without magnetic field. The lateral displacement of the spark[14] in chambers S_1-S_4, due to the magnetic field and the electric clearing field, was as high as 4 mm, and has been taken into account in the analysis.

2.7 Data acquisition

A Hewlett-Packard 2116B computer (24K memory) was connected to the apparatus and worked under the supervision of a Real-Time Executive operating system. Its main tasks were:

i) to read into the memory the relevant data of the events, namely spark coordinates and contents of scalers and pattern units, and to write the raw data onto magnetic tape;

ii) to construct and display histograms of the measured quantities;

iii) to reconstruct tracks for a sample of the events;

iv) to display a layout of the chambers with sparks and the reconstructed tracks on a memoscope;

v) to make periodic checks on the apparatus, i.e. on counters and trigger electronics;

vi) program development.

All these tasks competed for the central processor on the basis of a single scale of priorities. Hence all information on the experiment (tables, histograms, etc.) was available at any time during the data acquisition.

3. DATA HANDLING

The number of events collected with the elastic reaction trigger was 2×10^6 for the polarized target and 0.5×10^6 for the carbon target.

The off-line events reconstruction on the CERN CDC 7600 computer was performed in three steps:

i) geometrical reconstruction of tracks and selection of the events belonging to the elastic reaction trigger;

ii) fit of the negative pion trajectory through spark chambers S_1-S_8;

iii) selection of elastic events by calculation of the kinematical correlations.

3.1 Geometrical reconstruction of tracks

The track reconstruction program fitted a straight line in the two coordinate planes of chambers S_5-S_8. Events with more than one track inside the target fiducial

volume were rejected. Chambers S_1-S_4 were then scanned for at least one spark in S_1 and S_2, and one spark in S_3-S_4, which, coupled to the reconstructed track in S_5-S_8, would lie on a particle trajectory through the magnetic field. This search was done only in the horizontal coordinate plane, i.e. the plane perpendicular to the magnetic field. Only 40% of the events survived these preliminary requirements.

The events satisfying the elastic trigger condition were then selected and compacted on DST, with the additional condition that the backward particle has a negative charge. This condition only reduced the number of events by 15%.

3.2 Fit of the trajectory

The trajectory parameters in the horizontal plane (direction outside the magnetic field and momentum) were then fitted by a program which looked for the best trajectory through the coordinates of all sparks in S_1-S_8. A fast routine was developed which parametrized the trajectory in the highly inhomogeneous magnetic field as a function of three parameters: distance of the trajectory from the magnet centre; its intersection with a circle of 1.2 m diameter (outside the magnetic field); and particle momentum. The routine, which took full advantage of the azimuthal symmetry of the magnetic field, calculated the coordinates of the trajectory at the spark chambers. The trajectory parameters were then computed by minimizing the χ^2 constructed with the measured coordinates and the calculated intersections. The error correlations due to multiple scattering were taken into account.

3.3 Kinematical reconstruction

The presence of a strong and very inhomogeneous magnetic field in the target region complicates the kinematical correlations between measured directions and momentum. We tabulated the values of the relevant kinematical variables, such as invariant square momentum transfer u, momentum of the scattered pion, direction of the recoil proton, as a function of the direction of the scattered pion outside the magnetic field, since this was the quantity measured with the best accuracy. The expected value of a given variable was then calculated on an event-by-event basis with an interpolation procedure.

3.3.1 Vertex reconstruction

We calculated the vertex coordinates z (along the beam direction) and y (vertical) by tracking back the fitted pion trajectory into the target region. Figure 5 shows the distribution of z for a subset of the events. The positions of the target, the cryostat walls, and the counters are indicated as well. In the final data sample, a cut was applied to select only events inside the target.

The vertical distribution of the vertex indicates full containment of the beam within the target.

3.3.2 Momentum correlation

For every event we computed $\Delta p/p = (p_{meas} - p_{calc})/p_{calc}$. Figure 6 shows the distribution of $\Delta p/p$ for events which satisfy coplanarity and angular correlation and originate from inside the PT. The width of the peak is 7% FWHM, and it is virtually constant over the whole range in u. Figure 7 shows, for comparison, the distribution of $\Delta p/p$ for all events coming from the target. The cut-off at negative values of $\Delta p/p$, corresponding to momenta much smaller than that of the elastic reaction, is due to the fact that particles emitted from the target with momenta lower than $\sim$ 100 MeV/c were trapped inside the magnetic field.

By selecting only those events with $|\Delta p/p| \leq 8\%$ we rejected more than 97% of the total background. This rejection power is due to the fact that most of the background is associated with inelastic reactions on free and bound nucleons, characterized by a final state with a missing mass to the detected negative pion that is larger than the proton mass. Events with momentum higher than that for the elastic reaction are instead coupled to a missing mass lower than the proton mass, and are therefore only explained by assuming an elastic interaction taking place on a moving nucleon in a nucleus.

3.3.3 Angular correlation

The expected intersection of the forward proton trajectory with the vertical hodoscope R_2 was calculated from the scattered pion direction, and was compared with the position of the scintillator strip which gave signal. The distance between these two positions, expressed in millimetres, has been taken as a measure of "angular correlation". Figure 8 represents a plot of angular correlation for events satisfying momentum correlation and coplanarity in a u-bin $-0.43 < u \leq -0.19$ GeV^2. The elastic peak is clearly seen and has a width of 35 mm FWHM, fully compatible with the expected resolution. It is mainly due to the horizontal divergence of the beam and the finite width of the hodoscope elements.

3.3.4 Coplanarity

The bending of particle trajectories due to the vertical and radial components of the magnetic field caused a deviation from tight coplanarity between the directions of the incident particle and the scattered particles measured outside the magnetic field. We have therefore tracked back the particle trajectories into the target and defined the coplanarity parameter as the difference between the azimuthal angles in the target of the forward- and backward-scattered particles.

The distribution of coplanarity for events with $-0.43 < u \leq -0.19$ is shown in Fig. 9. The FWHM of the distribution varies between 3° and 4° over the whole

u-range covered, and is the value expected from the R_3 hodoscope bin width (2°) and the vertical beam divergence.

3.4 Selection of elastic events and normalization

In order to select the elastic events, cuts were applied to the $\Delta p/p$, coplanarity, and angular correlation distributions.

The background under the elastic peak has been evaluated (and checked) in the same way as in the previous experiment[1]. A preliminary cut in $\Delta p/p$ eliminated nearly all the background due to interactions on free (and polarized) protons. What was left were the elastic events on free protons and background events on bound (and therefore unpolarized) protons. The background present under the coplanarity and angular correlation peaks has been evaluated by assuming that the shape of the coplanarity distribution of background is the same for events inside and outside the angular correlation peak.

The background has therefore been calculated by multiplying the coplanar events outside the angular correlation peak by a normalization factor, which was estimated from the non-coplanar events.

This procedure of evaluating the background has been checked with the data taken with the carbon target, but has been preferred to the latter because it is statistically more precise.

The number of events left after background subtraction was 1800. The signal over background ratio varied from 1.5 to 3.5. Figure 10 shows the coplanarity distributions for elastic events in the bin $-0.69 < u \leq -0.82$ GeV^2 separately for target polarization along (up) and against (down) the magnetic field. The number of events with target polarization "up" and "down" have been normalized by using the events produced in the cryostat walls and in the counters B_4 and R_1, with a statistical accuracy of $\sim$ 1%. Any other "internal" determination of the normalization factor agreed with this one within statistical errors, and we chose the value which had the smallest statistical error.

4. RESULTS AND DISCUSSION

The measured values of the polarization parameter are given in Table 1 and shown in Fig. 11. The errors given are statistical only. Over-all systematic errors due to the measurement of target polarization and to the evaluation of the up-down normalization factor are estimated to be $\leq$ 5%. We have checked the compatibility of our results with the existing pion-proton cross-section[3-5] and polarization[1] data at this energy, using isospin inequalities applied to polarizations[16]. Owing to the actual value of the phase difference between the $I_u = \frac{1}{2}$ and $I_u = \frac{3}{2}$ exchange amplitudes[17], we obtain typically in this u-range the

inequality $-2.3 \leq P^- \leq 1.2$. This result only shows that these limits are compatible with any value of P^-.

4.1 Comparison with data at 6 GeV/c

If we compare these data with those at 6 GeV/c, we see that there is a large variation of the polarization with energy. Data at lower energy[8] also show rapid variations of polarization: in particular, for $u \simeq -0.7$ GeV^2, P changes sign twice from 2.93 to 6.0 GeV/c. This can be contrasted with the situation for the π^+p scattering at 3.5 and 6.0 GeV/c, where P varies very little. This difference in behaviour might hint at a greater importance of s-channel resonances in determining the backward scattering amplitude for the π^-p than for the π^+p reaction. If, however, we compare the 180° cross-section data for the two reactions[18], we see that in both cases resonances still manifest themselves, in the energy region between 3 and 6 GeV/c, as small oscillations of the cross-sections superimposed on a larger contribution smoothly decreasing with energy. It is therefore difficult to see how the very small contribution of resonances, which does not affect the polarization in the π^+p reaction, can produce the drastic change in the polarization of the π^-p reaction from -0.2 to +0.5, which is seen for $u \leq -0.6$ GeV^2.

In a Regge theory framework, it could be concluded that 3.5 GeV/c is too low a momentum, and that measurements at this energy do not belong to the high-energy region. Since, however, Regge parametrization of pion-nucleon backward scattering amplitudes fails completely to describe polarization data, we cannot draw any conclusion about "Regge threshold" from the difference between the π^-p data at 3.5 and 6.0 GeV/c. In fact, the naive Regge model would have predicted zero polarization in π^-p scattering, as only one trajectory, Δ_δ, is exchanged.

It is true, however, that, if we define a kind of "experimental asymptotics" in which cross-sections decrease smoothly with energy according to a power law s^{-n}, and polarizations stay constant or also decrease steadily with a power law of s, we can conclude that π^+p backward data are already asymptotic at 3.5 GeV/c [1], while the π^-p data at 3.5 GeV/c are not.

4.2 Separation of isospin ½ (N) and ³⁄₂ (Δ) exchanges

At this energy we have performed the same model-independent analysis of pion-proton backward scattering that Barger and Olsson[6] have done at 6.0 GeV/c. Since the amplitudes for the backward-scattering processes $\pi^-p \to p\pi^-$, $\pi^-p \to n\pi^0$, and $\pi^+p \to p\pi^+$ are linear combinations of two pure isospin exchange amplitudes, which can be called, with obvious notation, A_N and A_Δ, one can separate the contributions of these amplitudes to differential cross-sections and polarizations by combining existing data on $d\sigma^-$ [3], $d\sigma^+$ [3,4], $d\sigma^0$ [5], P^+ [1] and P^-.

In particular, the Δ-exchange amplitude is automatically isolated by the fact that it is the only amplitude involved in the $\pi^- p \to p\pi^-$ process. The differential cross-section $d\sigma_N$ defined as the square of the amplitude A_N can be calculated exactly using existing values of $d\sigma^+$, $d\sigma^-$, and $d\sigma^0$. The calculated values are shown in Fig. 12, together with the (interpolated) values of $d\sigma_\Delta$. The data show that at this energy both cross-sections have a backward peak. Moreover, the $d\sigma_N$ shows the dip at $u \simeq -0.2$ GeV^2, which is also present in all higher energy data, and which, in a Regge exchange framework, is usually interpreted as a nonsense wrong signature zero of the N_α trajectory. The cross-section at the minimum is, however, different from zero, and in any case much larger than that due to the exchange of a Δ, thus indicating the presence of the exchange of another $I = \frac{1}{2}$ trajectory, besides the N_α. Lacking polarization data in the charge exchange reaction, it is not possible to calculate exactly the polarization P_N due to the interference of the A_N amplitude with itself. It is, however, possible to put limits on P_N using triangular inequalities[16]. The results of such a calculation are shown in Fig. 13. They prove that the large negative polarization found in the $\pi^+ p$ elastic scattering is due entirely to the N exchange, which result could anyway be expected from the fact that (Fig. 12) the A_Δ amplitude is much smaller than the A_N.

It is also interesting to note that, at variance with what happens at 6 GeV/c [6], at our energy the polarizations P^+ and P^- are significantly different in the $d\sigma^+$ dip region, i.e. at $u \simeq -0.22$ GeV^2. In fact in that region the $d\sigma_N$ is much larger than the $d\sigma_\Delta$, and so the amplitudes for the two charged reactions can be very different.

We are grateful to P. Dechelette and M. Renevey for technical assistance throughout the experiment, and to the Polarized Target Group, M. Borghini, J. Conciencia, H. Ponssen, J.M. Rieubland, F. Udo and G. Zambelli for the efficient target operation.

G. Petrucci, G. Pozzo and J. Van der Meulen modified the spectrometer magnet to adapt it to a Polarized Target operation.

We acknowledge the participation of G. Contento during the early stages of this work.

Table 1

Polarization in $\pi^- p$ scattering at 3.5 GeV/c

u (GeV^2)	cos θ_{cm}	P
-0.23 ± 0.04	-0.886 ± 0.014	0.05 ± 0.08
-0.31 ± 0.04	-0.858 ± 0.014	-0.07 ± 0.08
-0.39 ± 0.04	-0.830 ± 0.014	-0.19 ± 0.08
-0.495 ± 0.065	-0.794 ± 0.0225	0.18 ± 0.11
-0.625 ± 0.065	-0.749 ± 0.0225	0.52 ± 0.09
-0.755 ± 0.065	-0.704 ± 0.0225	0.51 ± 0.09
-0.885 ± 0.065	-0.659 ± 0.0225	0.51 ± 0.11

REFERENCES

1) F. Bradamante, S. Conetti, C. Daum, G. Fidecaro, M. Fidecaro, M. Giorgi, G. Kalmus, A. Penzo, L. Piemontese, P. Schiavon, D. Stairs and A. Vascotto, Nuclear Phys. B56, 356 (1973).

2) F. Bradamante, S. Conetti, C. Daum, G. Fidecaro, M. Fidecaro, M. Giorgi, G. Kalmus, A. Penzo, L. Piemontese, P. Schiavon, D. Stairs and A. Vascotto, Phys. Letters 44B, 202 (1973).

3) J. Banaigs, J. Berger, C. Bonnel, J. Duflo, L. Goldzahl, F. Plouin, W.F. Baker, P.J. Carlson, V. Chabaud and A. Lundby, Nuclear Phys. B8, 31 (1968) and B9, 249 (1969).

4) R.A. Sidwell, R.R. Crittenden, K.F. Galloway, R.M. Heinz and H.A. Neal, Phys. Rev. D 3, 1523 (1971).

5) C. De Marzo, L. Guerriero, C. Nicolini, J. Posa, E. Vaccari, F. Waldner, G.T.Y. Chen, C.R. Fletcher, R.C. Lanou Jr., J.T. Massimo, D.S. Barton, B.A. Nelson, L. Rosenson and R.E. Thern, Phys. Letters 56B, 487 (1975); and C. De Marzo, private communication.

6) V. Barger and M.G. Olsson, Phys. Rev. D 5, 2736 (1972).

7) L. Dick, Z. Janout, H. Äoi, C. Caverzasio, A. Gonidec, K. Kuroda, A. Michalowicz, M. Poulet, D. Sillou, D.G. Aschman, N.E. Booth, K. Green and C.M. Spencer, Nuclear Phys. B64, 45 (1973).

8) P. Auer, D. Bridges, T. Droege, D. Hill, R. Giese, R. Miller, K. Nield, P. Rynes, B. Sandler, A. Yokosawa, G. Hicks, D. Miller and C. Wilson, Argonne preprint ANL-HEP-PR-75-65 (1975).

9) L. Dick, Z. Janout, H. Äoi, C. Caverzasio, A. Gonidec, K. Kuroda, A. Michalowicz, M. Poulet, D. Sillou, D.G. Aschman, N.E. Booth, K. Green and C.M. Spencer, Nuclear Phys. B43, 522 (1972).

10) V. Barger and D. Cline, Phenomenological theories of high-energy scattering (Benjamin, Inc., New York, 1969).

11) D.J. Sherden, N.E. Booth, G. Conforto, R.J. Esterling, J. Parry, J. Scheid and A. Yokosawa, Phys. Rev. Letters 25, 898 (1970).

12) E.L. Berger and G.C. Fox, Nuclear Phys. B26, 1 (1970).

13) W. de Boer, Nuclear Instrum. Methods 107, 99 (1973).

14) F. Bradamante, S. Conetti, C. Daum, P. Dechelette, G. Fidecaro, M. Fidecaro, M. Giorgi, A. Penzo, L. Piemontese, M. Renevey, P. Schiavon and A. Vascotto, Nuclear Instrum. Methods 116, 541 (1974).

15) F. Bradamante, S. Conetti, C. Daum, G. Fidecaro, M. Fidecaro, M. Giorgi, A. Penzo, L. Piemontese, P. Schiavon and A. Vascotto, Nuclear Instrum. Methods 112, 513 (1973).

16) L. Michel, Nuovo Cimento 22, 203 (1961).
G.V. Dass, J. Froyland, F. Halzen, A. Martin, C. Michael and S.M. Roy, Phys. Letters 36B, 339 (1971).

17) J.K. Storrow and G.A. Winbow, Nuclear Phys. B53, 62 (1973).

18) S.W. Kormanyos, A.D. Krisch, J.R. O'Fallon, K. Ruddick and L.G. Ratner, Phys. Rev. 164, 1661 (1967).
A.J. Lennox, W.F. Baker, D.P. Eartly, P. Koehler, J.A. Poirier, K.P. Pretzl, S.M. Pruss, C.A. Rey, O.R. Sander and A.A. Wehmann, Phys. Rev. D 11, 1777 (1975).

Figure captions

Fig. 1 : Layout of the experiment.

Fig. 2 : Close-up of the target region, showing the scintillation counters B_3, B_4, B_5, R_1, and M_1, and the cylindrical spark chambers S_1-S_4.

Fig. 3 : Magnetic field in the median plane as a function of distance from magnet centre. Positions of spark chambers are also indicated.

Fig. 4 : Scintillator R_2 and its coded light-guide system. The PM on lower left side defined the "high $|u|$" angular region.

Fig. 5 : Target profile along the beam direction, from a subset of data.

Fig. 6 : Distribution of $\Delta p/p$ for events inside the target and satisfying coplanarity and angular correlation.

Fig. 7 : Distribution of $\Delta p/p$ for all events inside the target.

Fig. 8 : Distribution of angular correlation for events inside the target, and inside $\Delta p/p$ and coplanarity peaks $-0.19 < u \leq -0.43$ GeV^2.

Fig. 9 : Distribution of coplanarity for elastic events in the bin $-0.19 < u \leq -0.43$ GeV^2.

Fig. 10 : Distributions of coplanarity for target polarizations up (——) and down (----). Elastic events with $-0.69 < u \leq -0.82$ GeV^2.

Fig. 11 : Polarization of $\pi^- p$ backward elastic scattering at 3.5 GeV/c.

Fig. 12 : Differential cross-sections $d\sigma_N$ and $d\sigma_\Delta$.

Fig. 13 : Isospin bounds on polarization P_N due to interference of the $I_u = \frac{1}{2}$ baryon exchange amplitude with itself. The values for P^+ used to calculate the points at $u = -0.755$ and -0.885 GeV^2 have been taken from Ref. 7, under the assumption that the equality of P^+ at 3.5 and 6 GeV/c, verified until $u = -0.585$, holds also in its immediate neighbourhood.

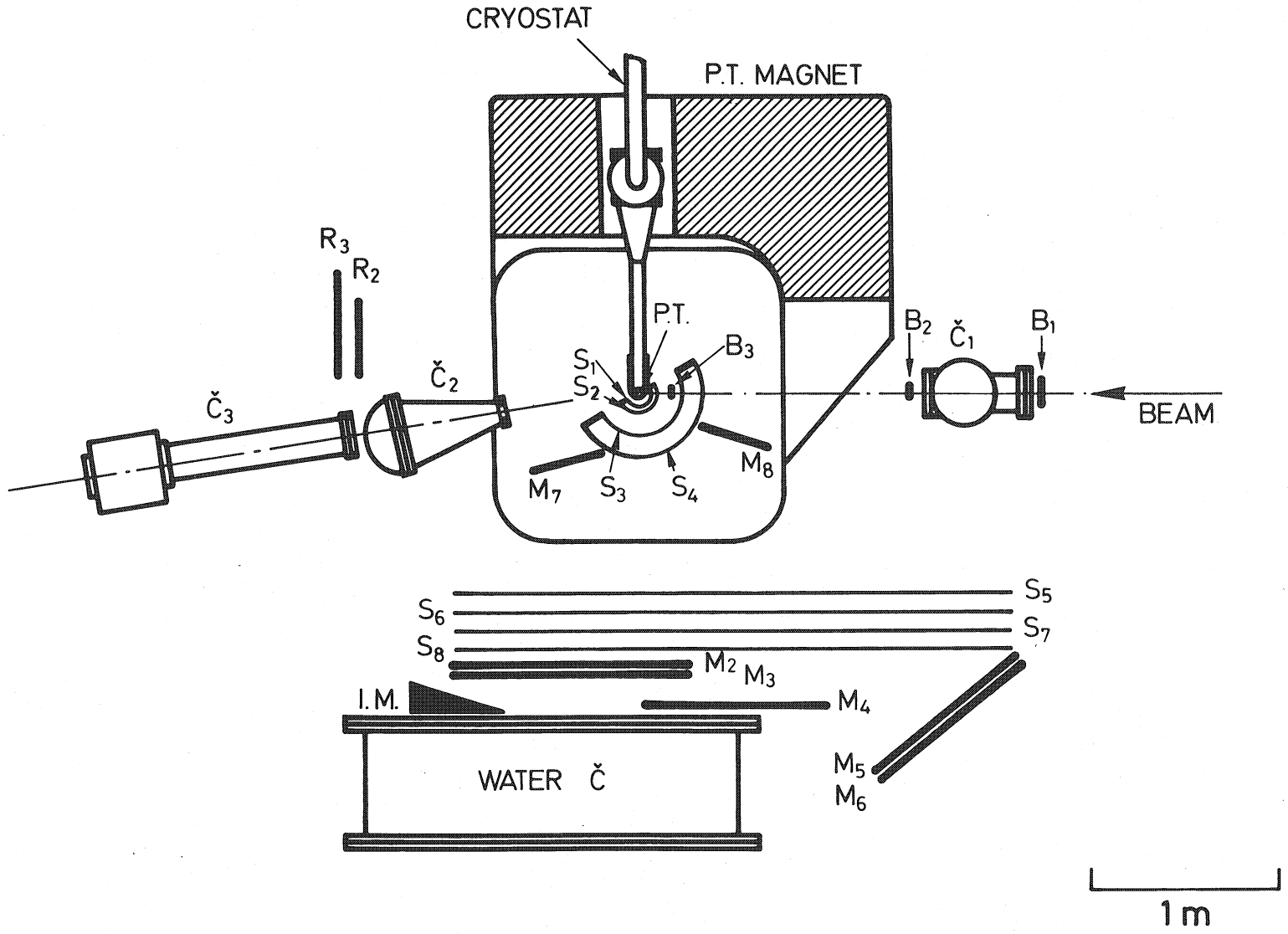
CRYOSTAT
P.T. MAGNET
R3
R2
P.T.
B2
Č1
B1
S1
B3
Č2
S2
Č3
BEAM
M7
S3
S4
M8
S5
S6
S7
S8
M2
M3
I.M.
M4
WATER Č
M5
M6
1 m

Fig. 1

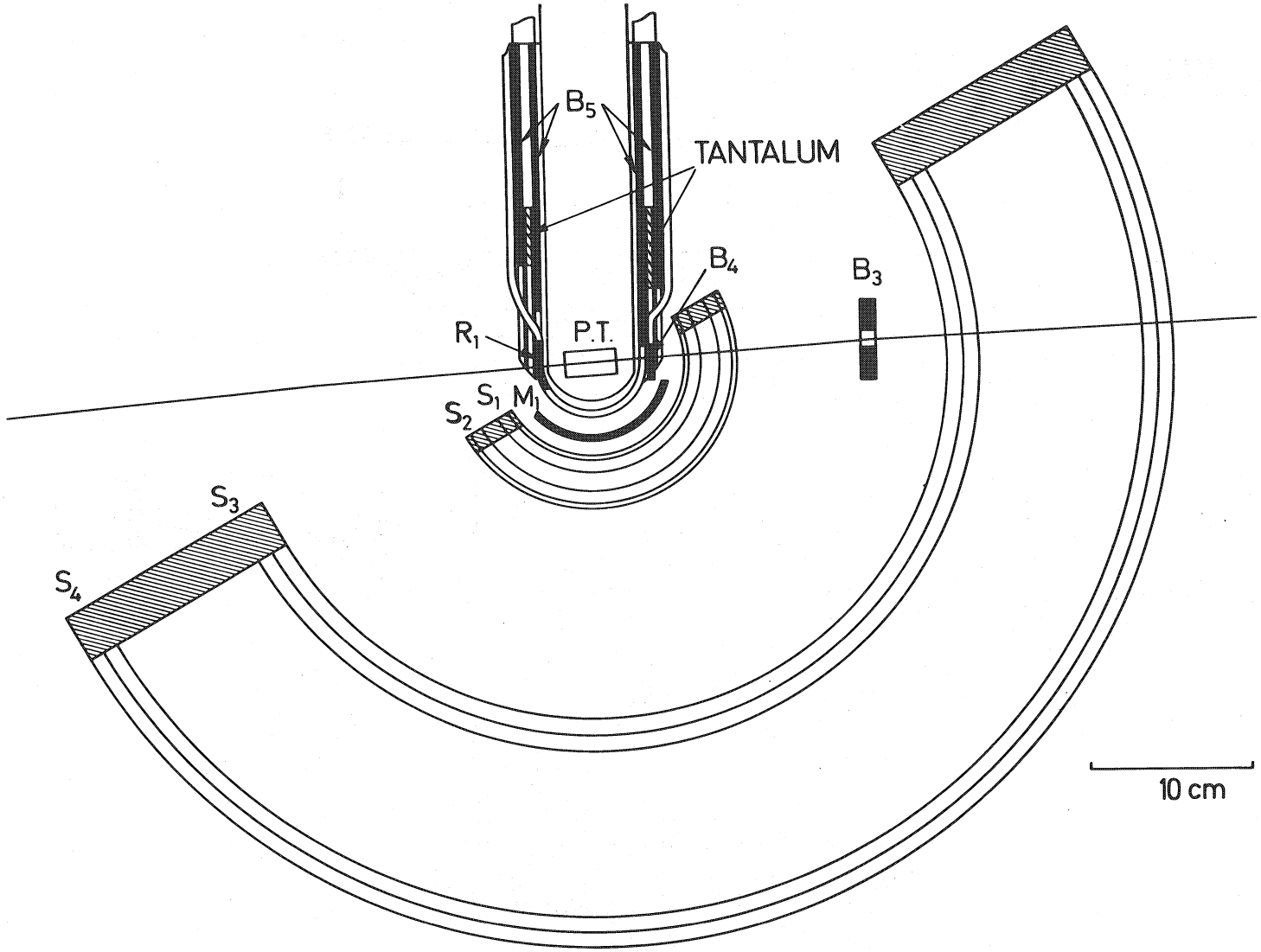

Fig. 2

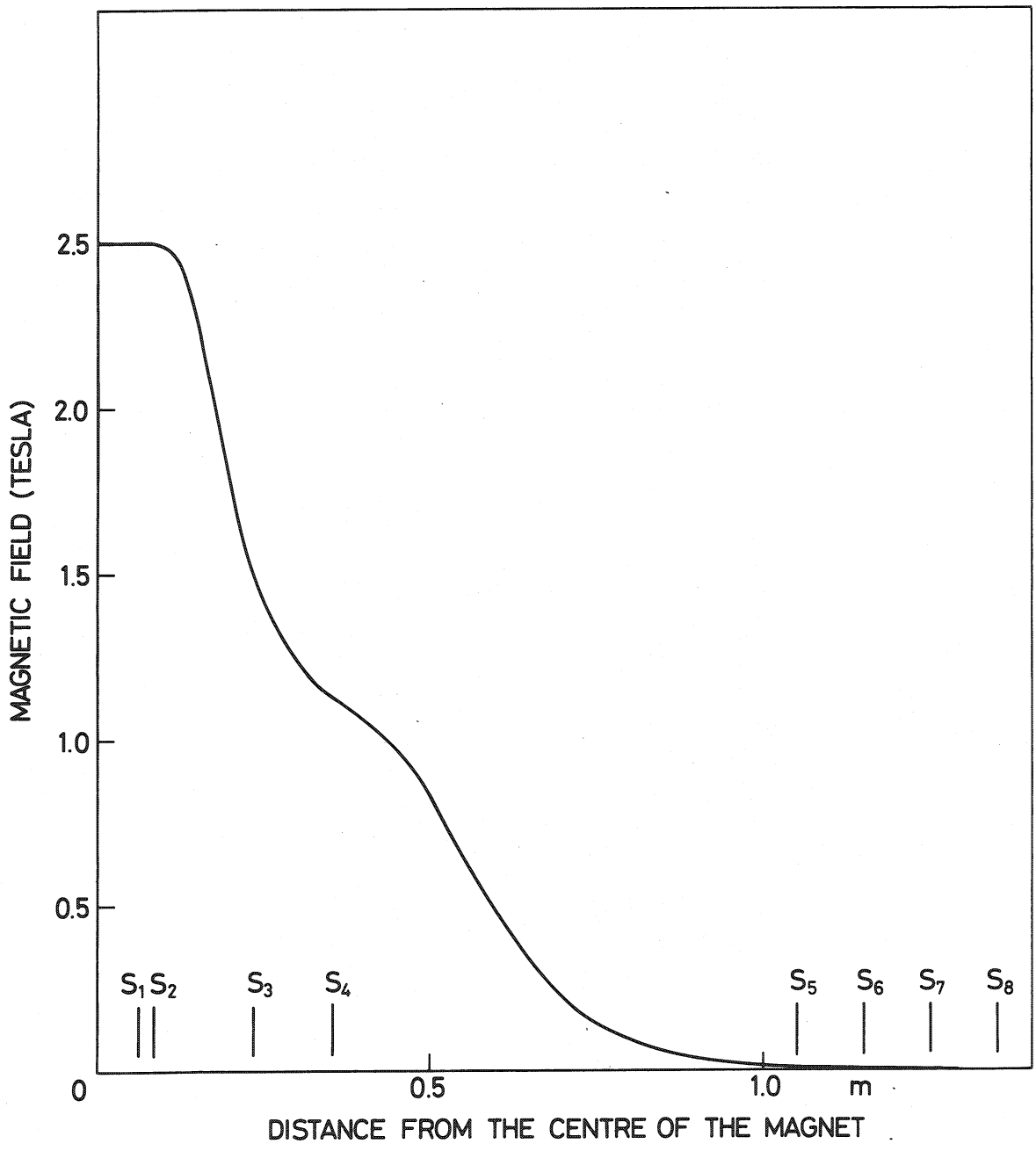
MAGNETIC FIELD (TESLA)
2.5
2.0
1.5
1.0
0.5
0
S1 S2
S3
S4
S5
S6
S7
S8
0.5
1.0
m
DISTANCE FROM THE CENTRE OF THE MAGNET

Fig. 3

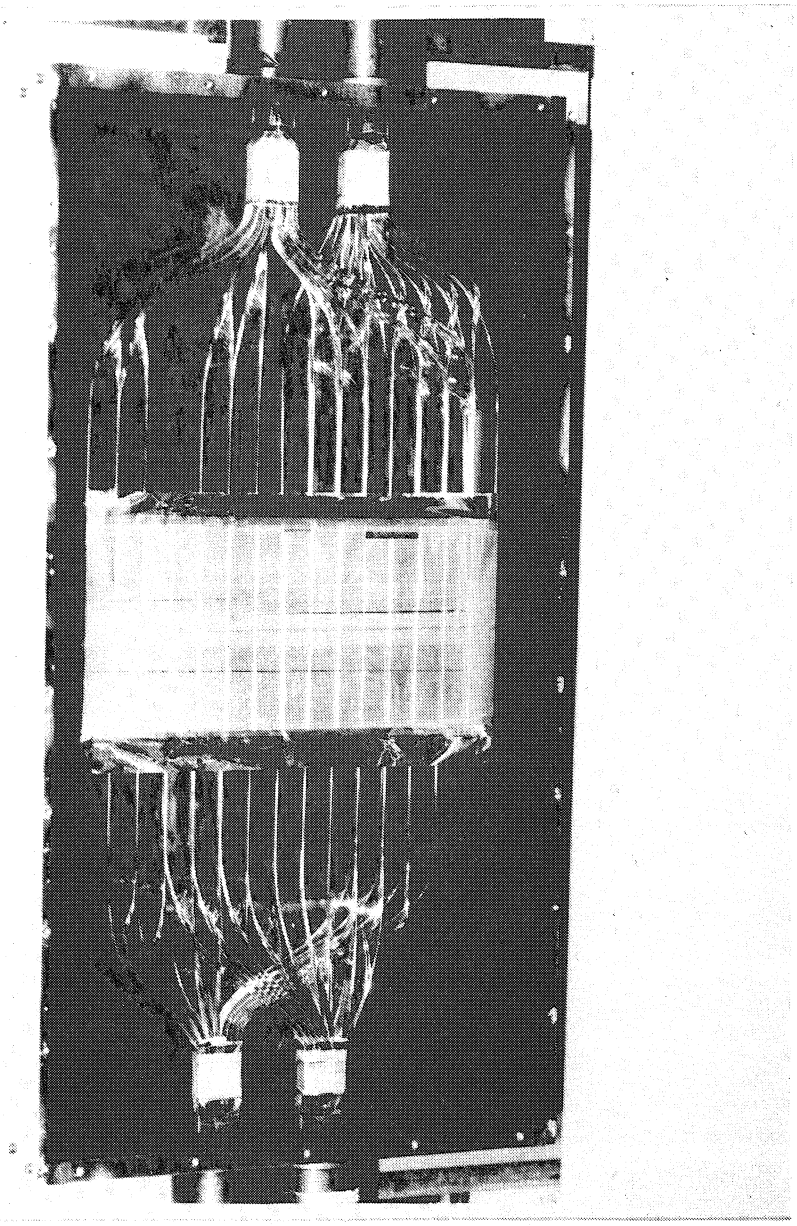

Fig. 4

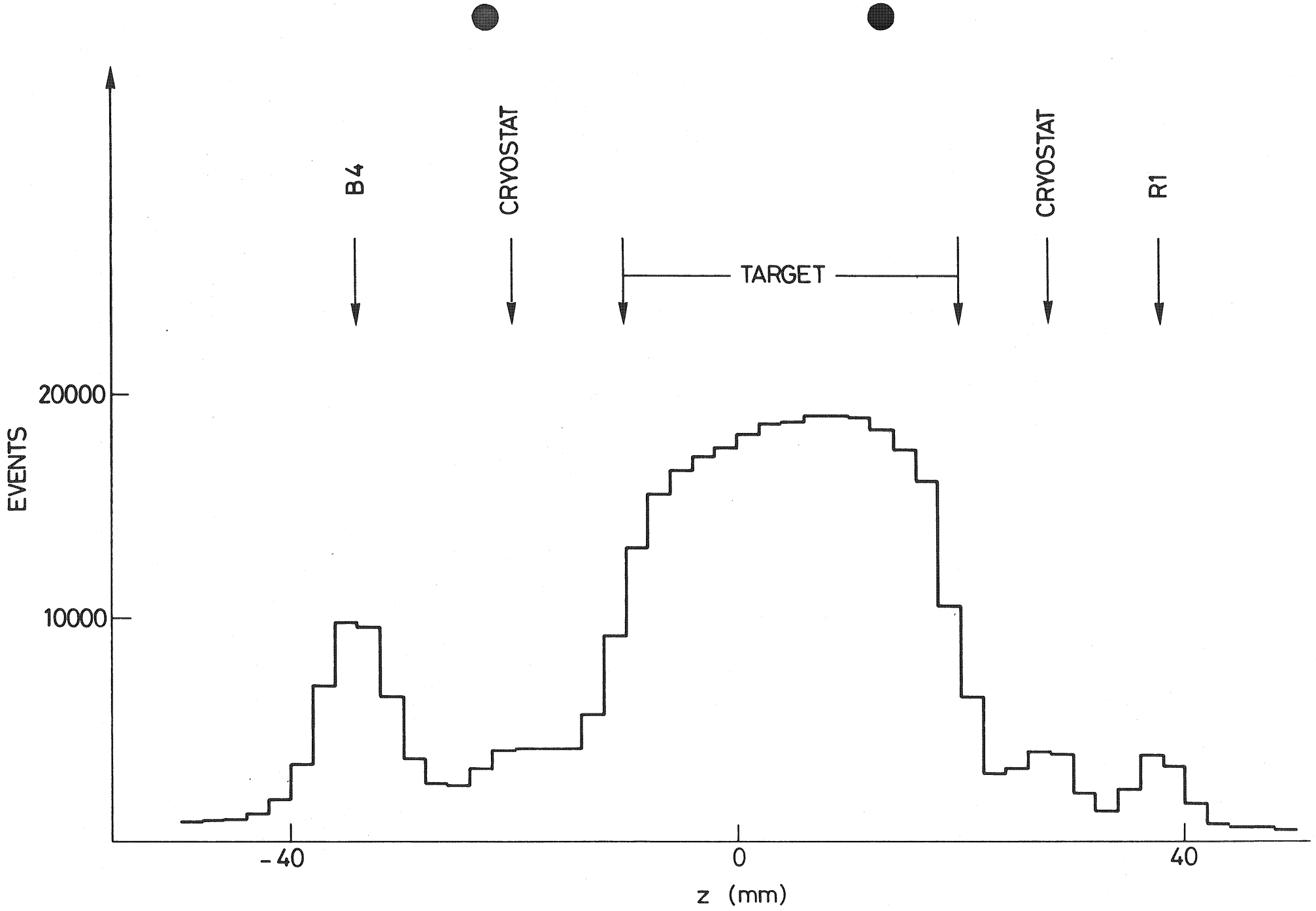
B4
CRYOSTAT
TARGET
CRYOSTAT
R1
EVENTS
20000
10000
-40
0
40
z (mm)

Fig. 5

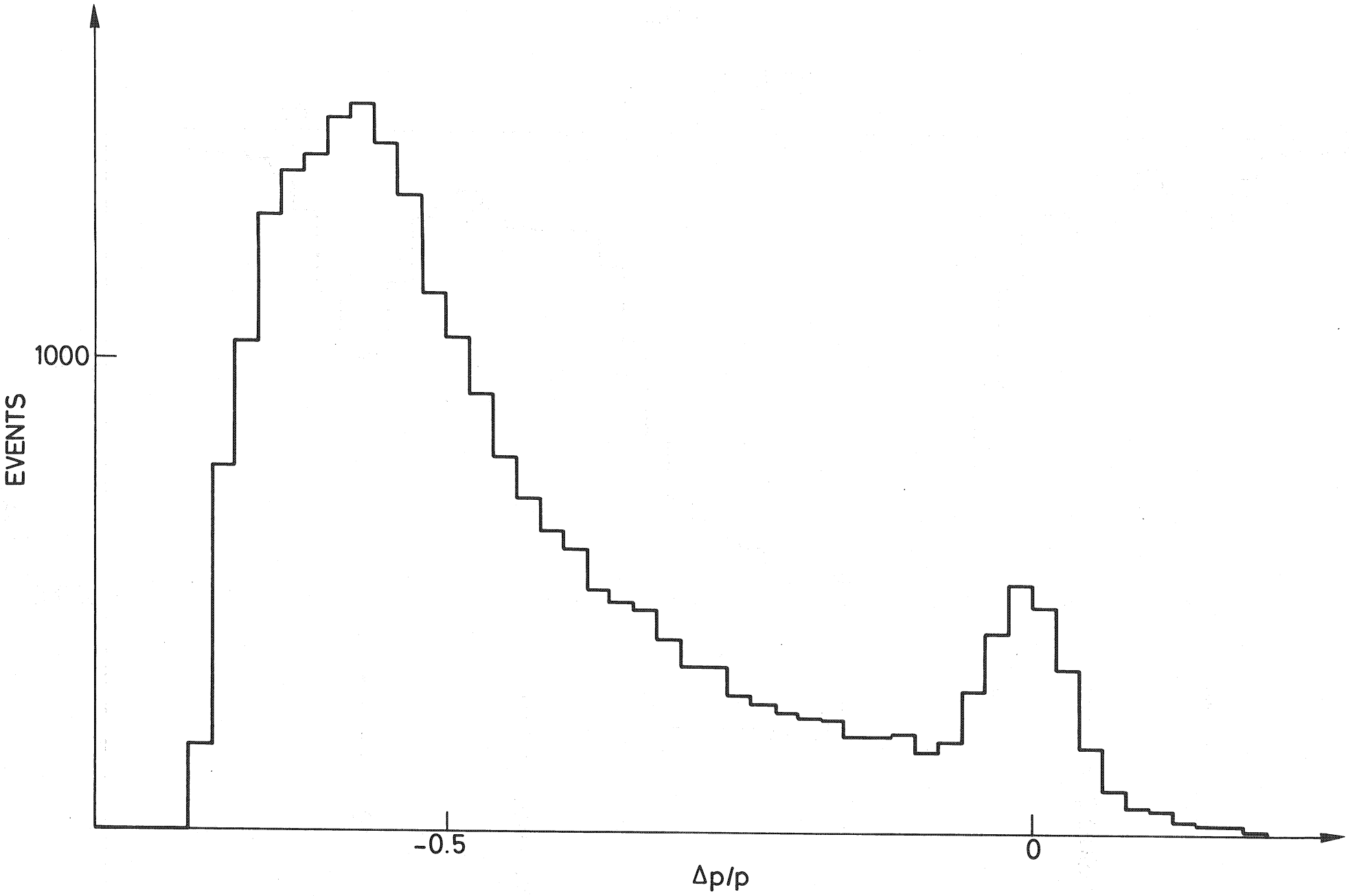

Fig. 6

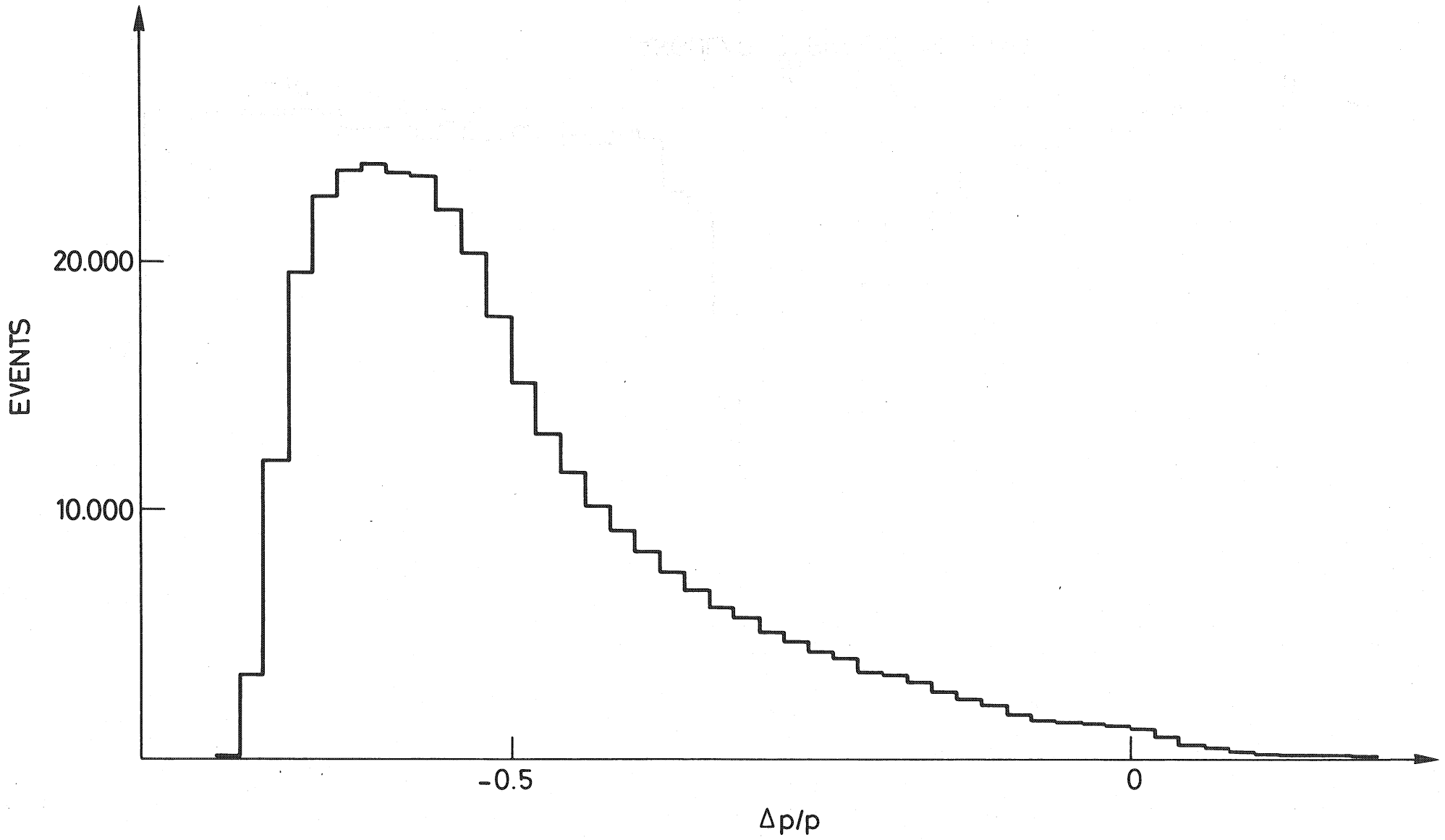

Fig. 7

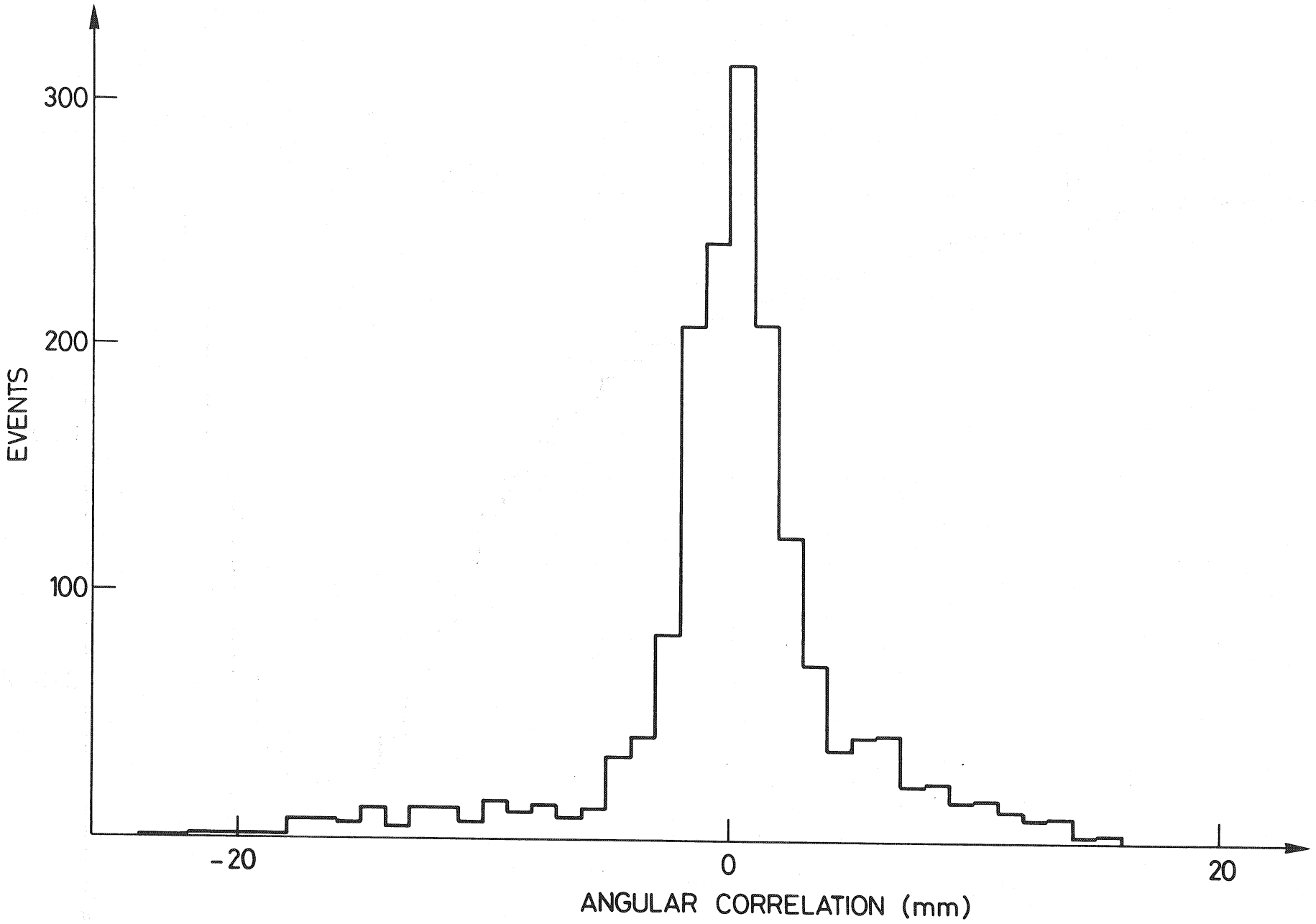

Fig. 8

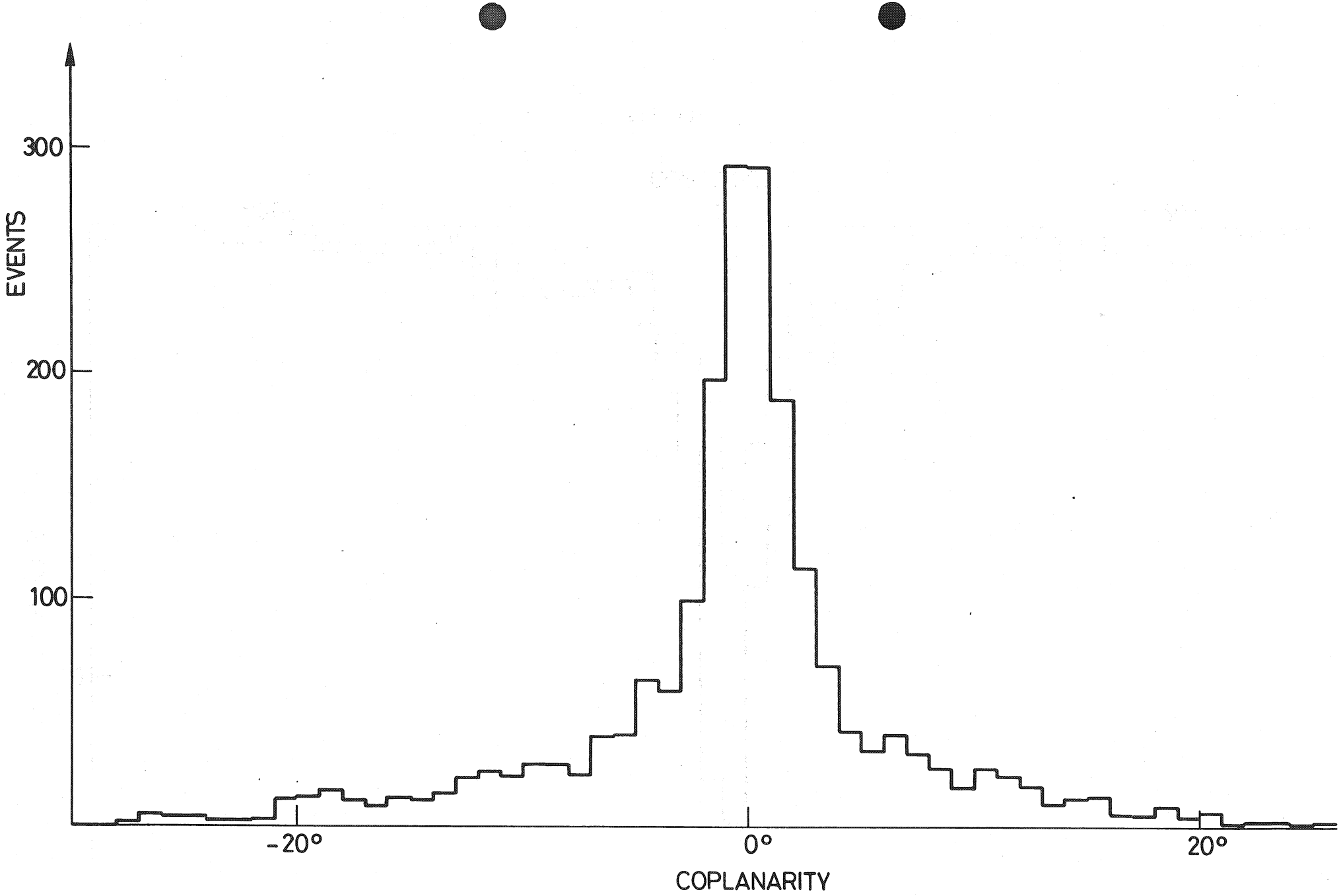

Fig. 9

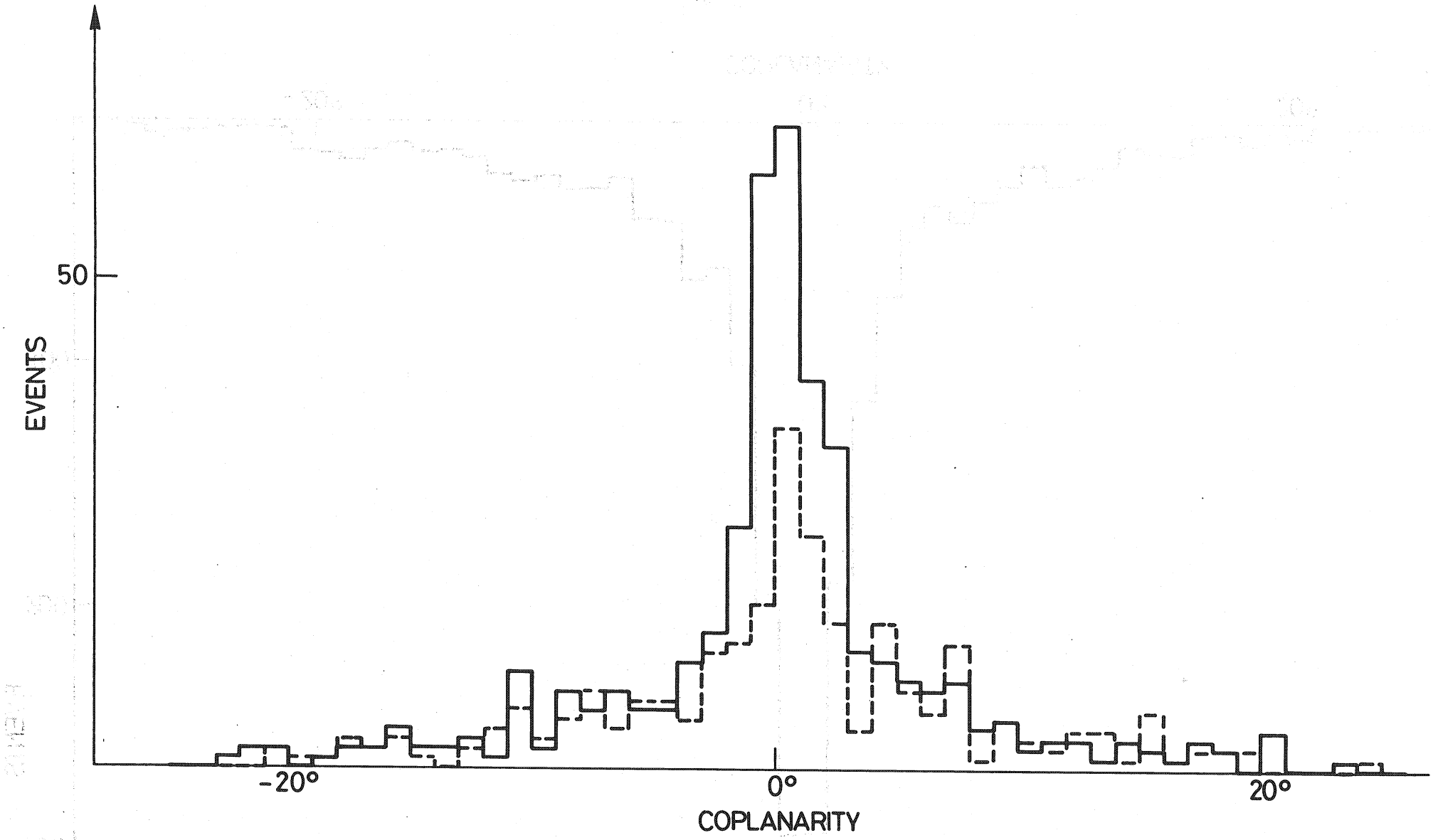

Fig. 10

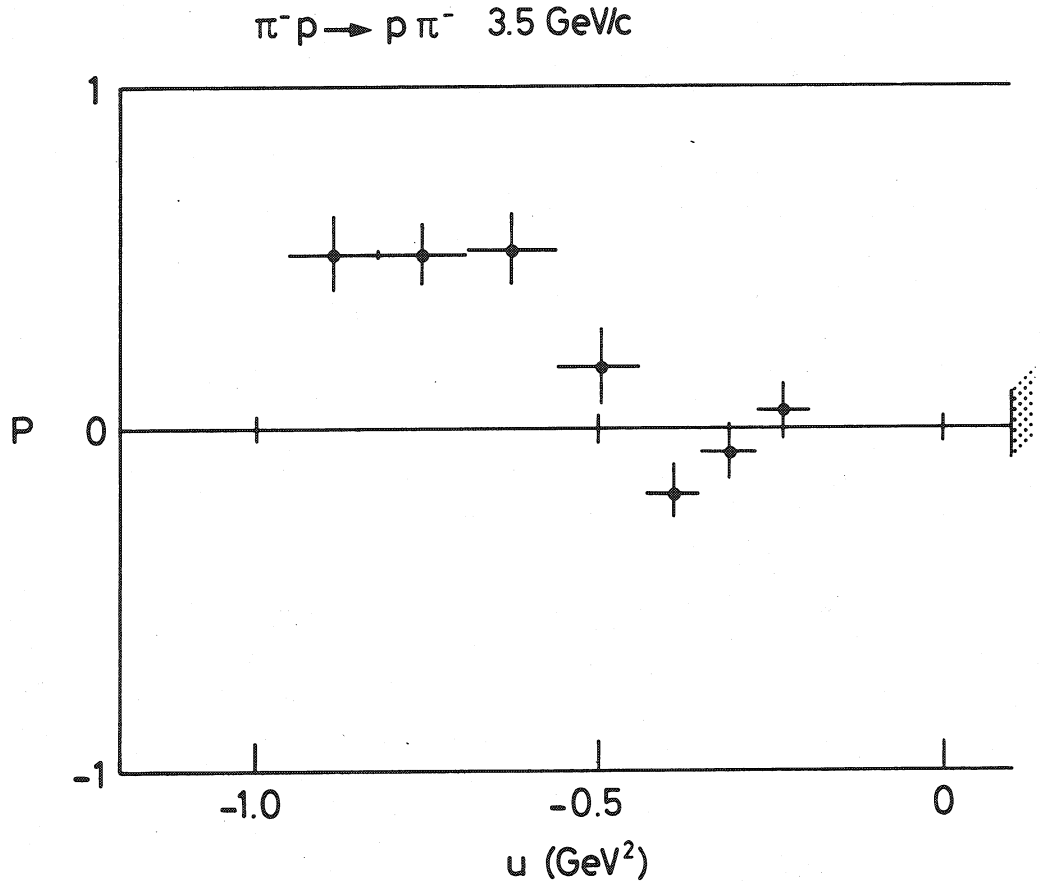

Fig. 11

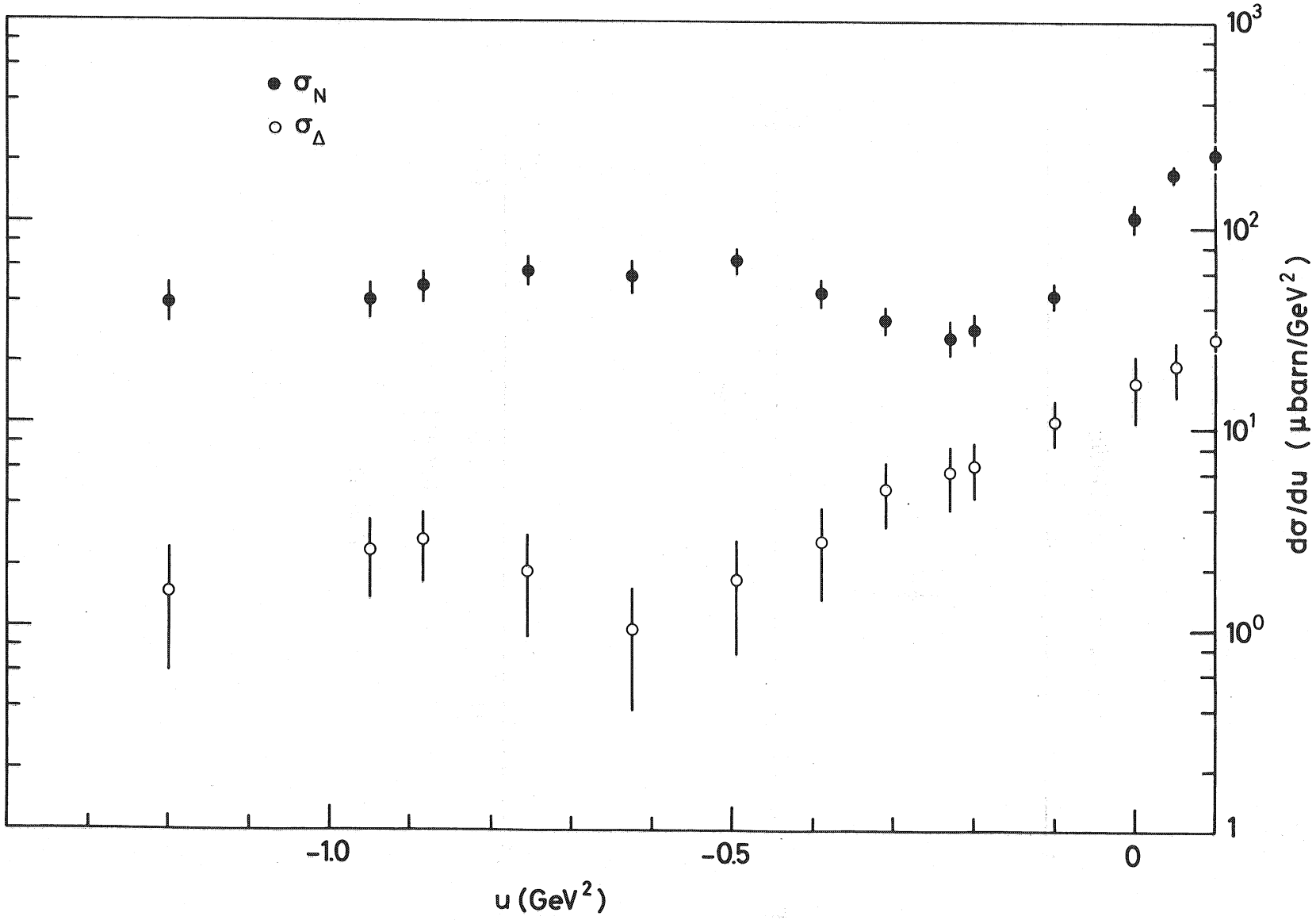
● σ_N
○ σ_Δ
10^3
10^2
10^1
10^0
1
$d\sigma/du$ (μbarn/GeV^2)
-1.0
-0.5
0
u (GeV^2)

Fig. 12

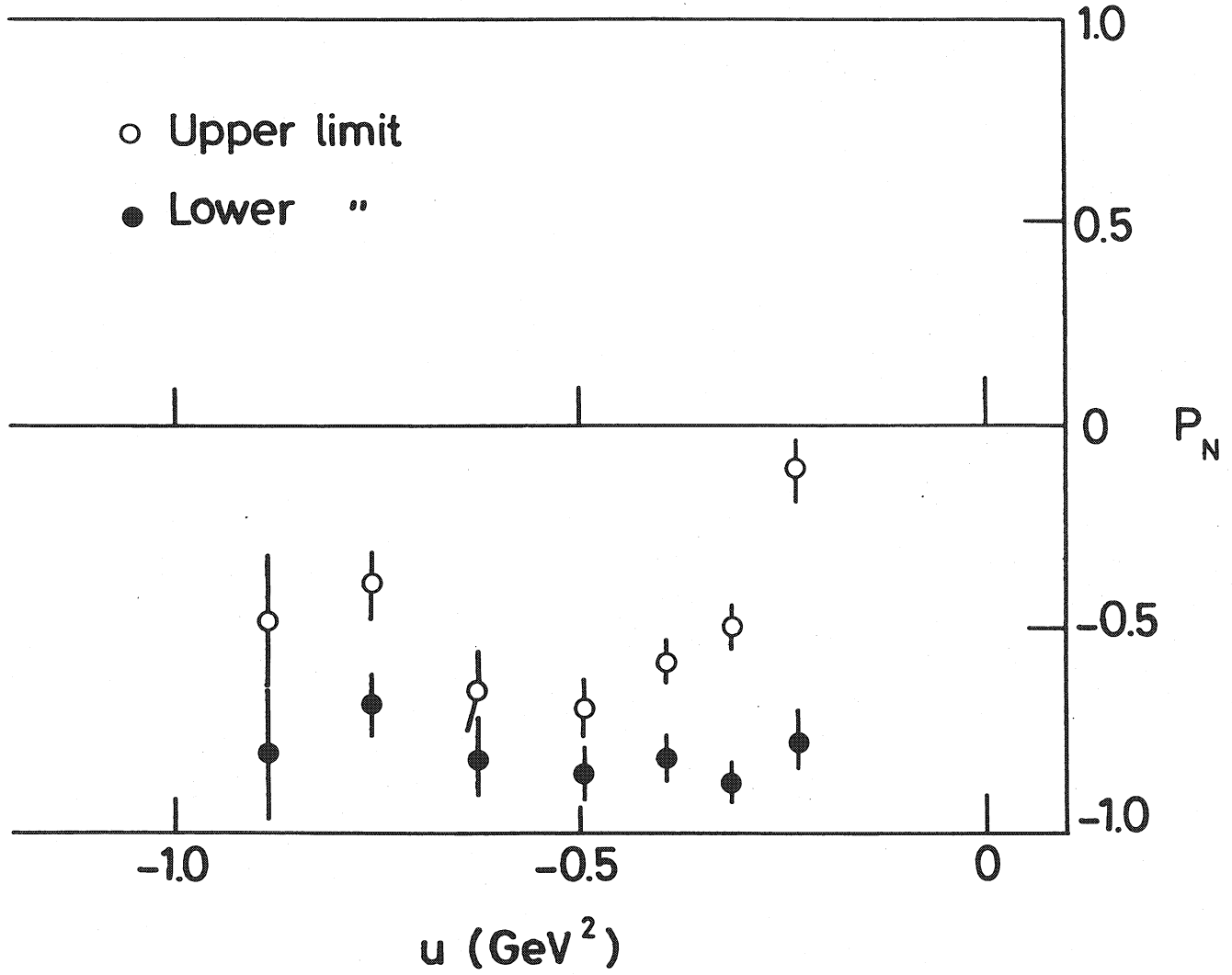

Fig. 13